JOURNAL OF PROPULSION AND POWER
Vol. 27, No. 3, May–June 2011

Effects of Orifice Internal Flow on Liquid Jets in Subsonic Crossflows

Jinkwan Song,* Kyubok Ahn,† Min-ki Kim,‡ and Youngbin Yoon§
Seoul National University, Seoul 151-742, Republic of Korea

DOI: 10.2514/1.B34011

The effects of orifice internal flow on the spray plume characteristics of the liquid jet injected perpendicularly into subsonic crossflows were investigated experimentally. The internal flows are classified into three modes: steady flow, cavitation flow, and hydraulic flip flow. These modes are mainly determined by the ratio of the injector length L to the injector diameter d and by the shape of the orifice internal edge. To study the spray plume characteristics corresponding to each mode, three measurement techniques were applied: mass-flow-rate measurement, direct photography of internal injector orifices, and planar liquid laser-induced fluorescence. From the results of the mass-flow-rate measurement and direct photography, each mode of orifice internal flow without air crossflow was classified through the discharge coefficient patterns and internal–external flow shape. Steady flow shows no significant change on the flow pattern, and the discharge coefficient increases as the pressure differential increases. However, unsteady flows, including cavitation and hydraulic flip, have strong bubble envelopes due to a sudden reduction of flow passage, and these phenomena affect the discharge coefficient patterns. The penetrations and the width of the liquid spray plume were analyzed using the images obtained from the planar liquid laser-induced fluorescence method, and they were compared with the previous results. The penetrations and width were formulated with the liquid–air momentum flux ratio q and the ratio of the distance from the injector exit to the injector diameter x/d. It is found that the spray plume trajectory is determined by the liquid column diameter of the orifice exit and the liquid–air momentum flux ratio using the jet velocity at the orifice exit. It is also found that it is better to use the nominal parameters in the case of cavitation flow, and it is better to use the effective parameters in the case of hydraulic flip flow.

Nomenclature

A	=	orifice area
C, c	=	constants
C_c	=	cavitation coefficient
C_d	=	discharge coefficient
d	=	orifice diameter
K	=	cavitation number
L	=	orifice length
$\dot{m}$	=	liquid mass-flow rate
P_v	=	vapor pressure
P_1	=	total pressure in the pressure vessel
P_2	=	ambient pressure
q	=	liquid–air momentum flux ratio, $\rho_f v_f^2/\rho_g v_g^2$
v_f	=	liquid velocity at orifice exit
v_g	=	gas velocity in airstream direction
x	=	distance in airstream direction
y	=	distance in direction transverse to airstream
z	=	distance in direction of width of spray
y_b	=	bottom height of spray distribution
y_m	=	maximum mass concentration height of spray distribution
y_t	=	top height of spray distribution
z_w	=	width of spray distribution
ρ_f	=	liquid fuel density
ρ_g	=	gas density in test section
P	=	injection pressure difference

Subscripts

cav	=	cavitation
eff	=	effective value
f	=	liquid property
g	=	gas property
hyd	=	hydraulic flip
j	=	jet property
non	=	noncavitation flow or steady flow

I. Introduction

FUEL injection and fuel–air mixing are important factors that determine engine performance. In particular, in airbreathing engines using liquid fuels, atomization and evaporation processes are required between fuel supply and combustion. Owing to the addition of these processes, it is difficult to provide a uniform and stable spray distribution temporally and spatially. Thus, it has become necessary to develop feasible fuel injection methods. The transverse method of injecting liquid fuel into the crossflow of the air is widely applied to airbreathing engines, including ramjet engines, scramjet engines, and turbojet augmenters. The transverse injection method is based on the liquid fuel–air momentum transfer at the surface of the liquid jet. When the liquid fuel is injected vertically into the crossflow of the air, aerodynamic acceleration occurs at the surface of the liquid jet, causing the liquid jet to bend the liquid fuel toward the leeward direction. Since a plain-orifice-type injector or hole in a wall surface is selected for the transverse injection, this injection method has little structural resistance, and the injection device is simple to produce. In this method, however, the spray distribution in the vertical direction is not uniform. Therefore, many researchers have recently investigated the transverse injection method to obtain a more accurate description of the spray characteristics caused by this method.

The spray distribution formed by the transverse injection of a liquid jet into the crossflow of air can be divided into three regions:

Presented as Paper 2007-5408 at the 43rd AIAA/ASME/SAE/ASEE Joint Propulsion Conference and Exhibit, Cincinnati, OH, 8–11 July 2007; received 11 May 2010; revision received 2 December 2010; accepted for publication 10 December 2010.

*Graduate Student, School of Mechanical and Aerospace Engineering.
†School of Mechanical and Aerospace Engineering; Researcher, Korea Aerospace Research Institute.
‡Graduate Student, School of Mechanical and Aerospace Engineering.
§Professor, School of Mechanical and Aerospace Engineering, San 56-1, Daehak-dong, Kwanak-gu; ybyoon@snu.ac.kr.

liquid column region, ligament region, and spray plume region [1]. In the liquid column region, the liquid jet sustains the nozzle shape of the injector after fuel injection. As the liquid fuel starts to break up, big drops (ligaments) and small droplets are formed in a jumble; this region is called the ligament region. After these ligaments disintegrate into tiny droplets, the spray plume region is formed, consisting of these tiny droplets.

Numerous studies have been carried out in order to understand the spray characteristics of the liquid column region, including the breakup mechanism, penetration, and trajectory. Schetz et al. [2] divided the liquid column waves into windward waves and leeward waves; the windward surface waves are developed from the acceleration of the liquid column surface caused by the aerodynamic drag force. Ingebo [3] investigated the capillary waves and acceleration waves in the liquid column region and found that ligaments are formed from the crest of the liquid column waves. These results show that the liquid column waves formed by the acceleration of the liquid column surface due to aerodynamic force are the major cause of the breakup mechanism of transverse injection. Schetz and Padhye [4] defined a penetration height as an asymptotic value as the jet lost its normal momentum; they measured the penetration height at 6.25 jet diameters downstream of the center of the injector and expressed it as a function of an injector diameter and a jet/freestream dynamic pressure ratio. According to Ingebo [5], maximum penetration can be explained as a function of $(Re_{fd}/We_{gd})^{0.7}$. Chelko [6] carried out a simple dimensional analysis and found that normalized jet penetration (y/d) is related to v_j/v_∞, ρ_j/ρ_∞, and x/d. Chen et al. [7] obtained the exponential functions that explain the liquid column region, ligament region, and spray plume region using the Mie-scattering method. They also performed particle image velocimetry (PIV) to measure the velocities of the droplets. Wu et al. [8] analytically solved the liquid column trajectories based on the assumption that liquid acceleration was in balance with the aerodynamic drag forces in the airstream direction; the liquid column could be modeled as a cylindrical fluid element with the diameter of the nozzle exit. They then formulated functions related to the breakup location of the liquid column as $x_b/d = 8.06 \pm 1.46$ and $y_b/d = 3.44\sqrt{q}$. Sallam et al. [9] performed the experimental investigation of the primary breakup of round nonturbulent liquid jets in gaseous crossflow and suggested qualitative similarities between the primary breakup of nonturbulent round liquid jets in gaseous crossflow and the secondary breakup of drops subjected to shock wave disturbances. Stenzler et al. [10] conducted the experiments using various simulant fuel, including distilled water, acetone, and 4-heptanone, and determined penetration from 2-D Mie-scattering images of the spray. The effect of the injection angle on the liquid column trajectory was reported by some researchers [11–13]. Baranovsky and Schetz [11] investigated this injection angle effect for the supersonic flow condition, and Fuller et al. [12] and Kim et al. [13] studied this effect for the subsonic flow condition. The preceding research was related to the liquid column characteristics and the stable condition of internal orifice flow.

The spray characteristics in the spray plume region are connected with those in the liquid column region. Moreover, these characteristics, including the drop size, width of the spray distribution, penetration, and trajectory, greatly affect the combustion property. As stated previously, Schetz and Padhye [4], Ingebo [5], and Chen et al. [7] summarized their studies about the liquid column region and their studies also include the spray characteristics in the spray plume region. Inamura and Nagai [14] studied the spray characteristics of a water jet with orifice diameters of 1 and 2 mm using sampling probe measurements and a phase Doppler particle analyzer (PDPA). Oda and Hiroyasu [15] used sampling probe measurements and the light scattering method to obtain the mass flux and size of the drops. They also created a breakup model based on linear wave analysis. Kihm et al. [16] obtained the drop size correlation using dimension analysis and confirmed it with the light scattering method. Wu et al. [1] studied the spray structure of the spray plume region and deduced the spray characteristics and flux following the centerline and the cross-sectional distribution of spray. These results on the spray plume region were also obtained for the stable condition of the internal orifice flow; that is, the effect of the internal orifice flow was not considered. However, as mentioned by Wu et al. [8], the effects of the internal orifice flow (for example, cavitation or hydraulic flip) can influence the spray characteristics.

Nurick [17] reported that cavitation does not occur if curvature r of the injector orifice entrance is over $0.14d$. However, when equipment like an engine is produced, its injector orifices are commonly blind drilled, making it difficult to obtain a satisfactory curvature of the injector orifice entrance [17]. Moreover, although the desired curvature is actually produced at the injector orifice entrance, the possibility of cavitation due to heterogeneous nucleation is always inherent because of the high injection pressure. In addition, if the orifice length-to-diameter ratio is less than 10, cavitation bubbles expand to the orifice exit and transform into the air tube having a smaller inner diameter than that of the injector orifice; this phenomenon is referred to as hydraulic flip. Taking this into consideration, Tamaki et al. [18] found that when the liquid flow was disturbed by increased cavitation inside the orifice, atomization of the liquid jet was considerably promoted and the breakup length became short. Ahn et al. [19] found that the cavitation or hydraulic flip effect influences the liquid column trajectory and breakup length. They proposed an introduction of the effective jet diameter and effective jet velocity for various spray conditions.

Therefore, the objective of this study is to confirm the spray characteristics of the liquid jet with subsonic crossflows and to investigate the effects of cavitation and hydraulic flip, especially on the spray plume structures. The spray characteristics, such as the trajectory and width of the spray plume, which are known to be important factors in designing an injector and a combustor, were

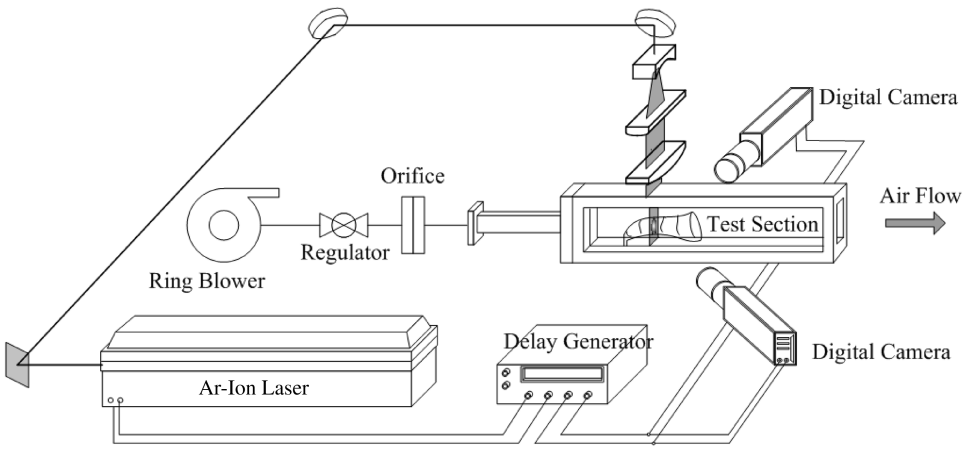

Fig. 1 Experimental setup for PLLIF.

measured by changing the orifice diameters, injector pressure differentials, and the shape (sharp and round) of the orifice entrance.

II. Experimental Apparatus and Condition

A. Experimental Apparatus

The experimental apparatus is composed as shown in Fig. 1. This apparatus consists of an air–fuel supply system, an injector, a test section, and measurement systems. For air supply, a 20 hp ring blower, which can supply a maximum airflow of 18 m^3/min, was employed. The air was supplied into the wind tunnel after it was passed through a honeycomb, and the uniform velocity profile of the inlet airflow was obtained. The fuel supply system comprises a fuel tank, a pressure-reducing regulator, and injectors. A fuel tank was pressurized with high-pressure air, and this pressurization was controlled by the regulator, which controlled the flow rate of the liquid. An electric heater and a proportional-integral-differential controller (Autonics TZ4ST) were installed inside the fuel tank to control the fuel temperature so that cavitation could be easily induced on the internal flow of injector. Fuel pressures and temperatures are measured using pressure gauge (OMEGA PGT-45B-150) and *k*-type thermocouples (OMEGA). The uncertainties of pressure and temperature measurements are less than 1%.

To visualize the inside of each injector, injectors were made with acrylic material. The inside of the injector consists of an internal chamber and an orifice (Fig. 2a). The orifice diameter of the injectors

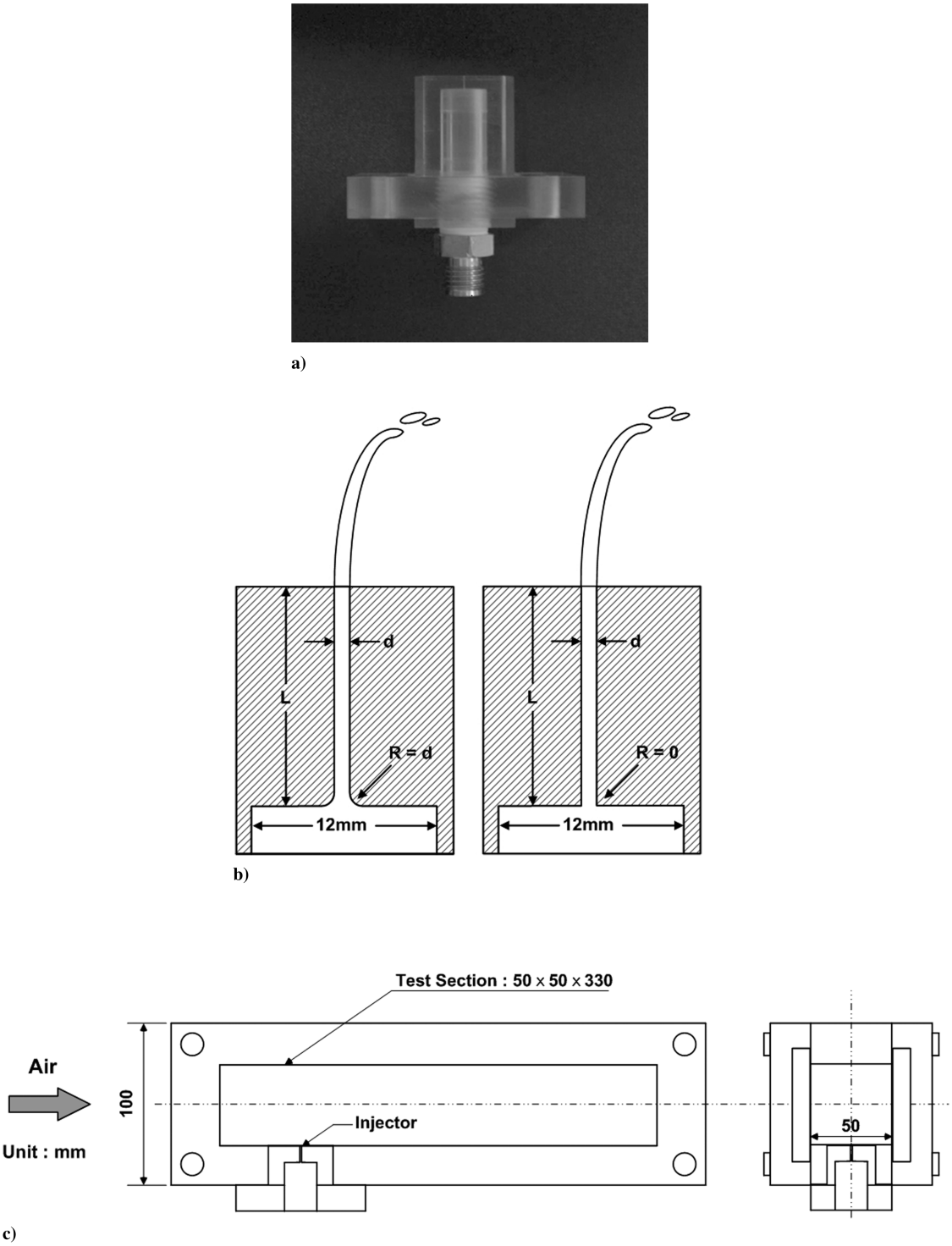

Fig. 2 Experimental apparatus: a) injector image, b) injector edge designs, and c) test section.

was 0.5 mm. For testing steady and cavitation flows, round-edged and sharp-edged orifices were designed at the entrance of the orifice and injectors with sharp-edged orifices were designed to have length-to-diameter ratios of 5 and 20, respectively, as shown in Fig. 2b. According to the previous result [17], the orifice that is rounded by 0.14 times of the orifice diameter or more has no vena contracta, and the length-to-diameter ratios of the injectors with sharp-edged orifices are important parameters for determining whether cavitation flow or hydraulic flow would occur. As shown in Fig. 2c, the test section has a rectangular cross section of 50×50 mm and a length of 330 mm. To visualize the spray structure, two windows were built on both sides of the test section. Acrylic windows were assembled as the top and the bottom walls of the test section. The bottom wall has a rectangular hole to permit injectors to be mounted, as shown in Fig. 2c.

Three kinds of experiments were performed: mass-flow-rate measurement, direct photography, and planar liquid laser-induced fluorescence (PLLIF). The discharge coefficient of each injector was calculated using the mass-flow-rate measurement results to assess the injector's characteristics. Typically, a discharge coefficient is defined by the following equation:

$$C_d = \frac{\dot{m}}{A\sqrt{2\rho_f \Delta P}} \tag{1}$$

The measured discharge coefficients contain many losses due to the cross-sectional reduction effect based on the boundary layer, liquid viscosity effect, surface friction effect, and so on. Therefore, it is widely used to elucidate flow phenomena. As the injection pressure differential varied from 1 to 6 bar with each injector, mass-flow rates injected within 30 s were measured.

We took photographs of the internal and external flows of the injector orifice and compared them between a stable flow pattern and an unstable flow pattern: that is, cavitation and hydraulic flip flow. Moreover, the outer jet diameters of each jet were measured to compare cavitation flow with hydraulic flip flow. At that time, a microcamera lens (Nikon 105 mm F2.8) and 3X teleconverter (Nikon) were mounted at the digital camera (Canon EOS D30, 12 bit, 2160×1440) to magnify the flows inside/outside the orifice. A strobe lamp (Sugawara) was used for the light source. The stroboscopic light, of which luminous time is less than 4 μs, is illuminated on the spray. If the velocity of a drop is 20 m/s, it moves just 0.08 mm during a flash time, and thus the spray image can be regarded as an instantaneous image. Also, the PLLIF method was performed. The planar fluorescent signals, which are excited by the specific wavelength laser beam, are obtained from the PLLIF method, and these signals depend on the concentration of fluorescing molecules [20,21]; the PLLIF method is a suitable method to measure the spray distribution. Using each injector, designed for stable flow, cavitation flow, and hydraulic flip flow, the PLLIF images for various liquid–air momentum flux ratios and distances to injector orifice in the downstream direction were obtained and analyzed. To produce a fluorescence signal proportional to the volume of the liquid, an ethanol–water solution of a 4:1 ratio containing 30 mg/l fluorescein dye (Aldrich F245-6, $C_{20}H_{12}O_5$) was used as the simulant fuel [22], because a fluorescence signal cannot be obtained when water is used as simulant fuel. The argon–ion laser (Spectra-Physics 2020, 3 W) with 514 nm wavelength was used to make the simulant fluoresced in the expected wavelength range. The beam lased from the argon–ion laser was changed into a sheet beam using fiber optics (Dantec). Fluorescence signals were measured with two digital cameras (Canon EOS D30, 12 bit, 2160×1440) that were mounted with a 550 nm high-pass filter. The physical spatial resolutions of images were about 62.5 μm per one pixel. The exposure time of the camera was less than 4.0 s with the laser power of 600 mW, which is believed to be adequate for the temporal average of sprays, and five images were averaged to represent one experimental case. The locations of the cameras were inclined with about 45° angles, as shown in Fig. 1, and the perspective errors of the images were corrected by an image processing known as an affine transformation [23]. To compensate for an incident laser attenuation, a geometric average method for the correction was used [24]. For these error corrections, the raw signal images were processed by the in-house code programmed with MATLAB 8.0. The uncertainty associated with PLLIF is estimated to be less than 5% when two cameras are used for the geometric average method [21,22,25].

Table 1 Experimental conditions

Parameter	Value
Air velocity	60 ± 1 m/s
Air temperature	300 K (27°C)
Fuel temperature	318 K (45°C)
Orifice diameter	0.5 mm
Orifice shape	Round-edged ($L/d = 20$), sharp-edged ($L/d = 5, 20$)
ΔP (bar)	1, 2, 3, 4, 5, 6
x/d	20, 40, 60, 80, 100, 120, 140, 160, 180

B. Experimental Conditions

Plain-orifice-type injectors of various orifice length-to-diameter ratios and orifice entrance shapes were created to investigate how the disturbance flow inside the orifice, caused by cavitation and hydraulic flip, influence the spray characteristics of the transverse injection in the crossflows of air. The orifice length-to-diameter ratios were 5 and 20, and the orifice entrance shapes of the injectors were designed as round edged and sharp edged, respectively. To change the liquid–air momentum flux ratio, air velocity was fixed to 60 ± 1 m/s and injection pressure differential is changed from 1 to 6 bar. In the PLLIF experiment, the spray distribution of the spray plume region is obtained as the measured cross section is moved by 10 mm, from 10 to 90 mm in the downstream direction. At the test section, the air velocity was confirmed by PIV. Air temperature was fixed to 300 K (27°C). For the test liquid, the ethanol–water mixture was used in the all measurements. The simulant fuel was heated to 318 K (45°C) so that the high vapor pressure would make it easy to produce cavitation or hydraulic flip. The simulant fuel density ρ_f, viscosity, and surface tension were 956.4 kg/m^3, 1.79×10^{-3} kg/m/s, and 37.22×10^{-3} N/m, respectively, and the fluorescein dye did not affect the physical properties of the simulant fuel [26]. Table 1 shows the dimensions of the orifice design parameters and experimental conditions.

III. Results and Discussion

A. Analysis of Internal Orifice Flows Using Mass-Flow-Rate Measurement and Photography

A mass-flow-rate measurement is a fundamental test that can assess an injector's performance. When an injector is designed for a desired mass-flow rate, a loss of mass-flow rate occurs due to many causes, such as surface friction and cavitation. The measurement of

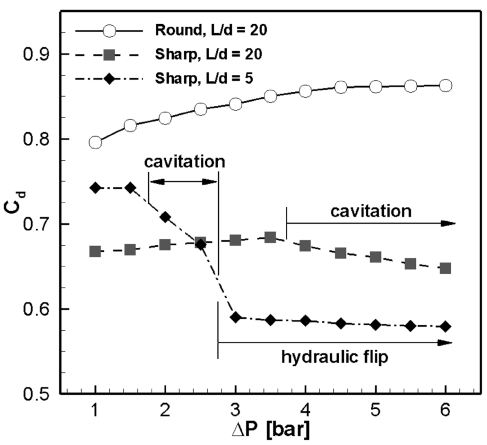

Fig. 3 Discharge coefficient of orifice diameter 0.5 mm as a function of injection pressure difference.

the actual performance of an injector should incorporate this loss. Figure 3 shows the discharge coefficients of each orifice for various injection pressure differential. The x axis indicates the injection pressure differential and the y axis indicates the discharge coefficient. For the round-edged orifice with the length-to-diameter ratio of 20 (0.5R injector), the discharge coefficient increases gradually in the pressure differential range below 4 bar and attains a constant value in the range of above 5 bar. When the pressure differential is low, the round-edged orifice has small coefficient values, because a considerable mass-flow loss occurs due to the friction from the orifice inner wall. However, as the pressure differential increases, the coefficient also increases. These results agree with the fact that the discharge coefficients linearly increase with respect to the Reynolds number [27]. In the case of injectors used to induce cavitation or hydraulic flip by changing the orifice length-to-diameter ratio and orifice entrance shape, contrary to the result of the former injector, we could observe different aspects. For the sharp-edged orifice with a length-to-diameter ratio of 20 (0.5S injector), the discharge coefficients showed almost the same tendency with those of the round-edged orifice up to 3.5 bar. However, when the flow passage suddenly reduces and the inflow experiences resistance at entrance edge due to the shape-edged orifice, the mass-flow rate of inflow then decreases. Hence, at the same pressure differential, the discharge coefficient of the 0.5S injector is smaller than that of the 0.5R injector. Above the pressure differential of 3.5 bar, the discharge coefficients decrease gradually due to cavitation. The vena contracta reduces the flow passage size, and air bubbles arising from cavitation decrease the inflow mass-flow rate. Thus, the discharge coefficient has a smaller value, as reported in Nurick [17]. In the case of the sharp-edged orifice with a length-to-diameter ratio of five (0.5SS injector), the discharge coefficient curve of this injector shows smaller values (as in the results of the 0.5S injector) than that of the 0.5R injector due to the decrease of the inflow mass-flow rate at the sharp-edged nozzle entrance. However, compared with the coefficient curve of the 0.5S injector, the curve of the 0.5SS injector shows larger values, because the mass-flow-rate loss related to wall friction reduces due to the short orifice length L. As the injection pressure differential increases and exceeds 2 bar, cavitation takes place, which fills the shortened orifice passage with cavitation bubbles. This phenomenon considerably decreases the mass-flow rate; thus, the curve shows smaller values than that of the 0.5S injector. As the injection pressure differential reaches 3 bar, cavitation bubbles expand to the orifice exit and transform into the air tube having a smaller inner diameter than that of the injector orifice; that is, cavitation changes into hydraulic flip. When hydraulic flip occurs, the liquid jet diameter becomes smaller than the injector orifice diameter. Moreover, even if the injection pressure differential increases, the discharge coefficient value remains constant (like the curve in Fig. 3), because the area of the flow passage surrounded by the air tube is unchanged. Generally, when a sudden area change in the flow path gives rise to a mass-flow limitation, the discharge coefficients of the round-edged orifice become larger than those of the round-edged orifices.

Pictures of the flow shape of the inside/outside of the orifice for each injector were taken based on these mass-flow-rate results. Using the obtained images of the internal and external flows, we observed the flow patterns of cavitation and hydraulic flip and compared the flow pattern results with the discharge coefficient results. Figure 4 shows the flow pattern photographs of the internal and external flows of each injector for various injection pressure differentials. For the 0.5R injector, the orifice internal flow remains unchanged, although the injection pressure differential increases. However, the jet flow outside the orifice becomes turbulent as white bubbles arise at the shear surface with the increase of the injection pressure differential. Because an increase in the pressure differential increases the injection velocity of the test fuel at the same injector orifice diameter, this jet flow result is caused by a strong turbulence that is related to the increase of the Reynolds number. On the other hand, the flow shape of the 0.5S injector shows a difference from that of the 0.5R injector. As mentioned in the discussion regarding the discharge coefficient, cavitation occurs in the injection pressure differential range of 3 to 4 bar. Before cavitation, there is no appearance of bubbles inside the orifice, like in the case of the 0.5R injector. When cavitation occurs, the length of the white bubble inside the orifice becomes longer as injection pressure differential increases. However, cavitation does not transform to hydraulic flip, because the orifice length in the case of the 0.5S injector is so long that cavitation expands to the orifice exit. Typically, it has been reported that hydraulic flip does not occur if the orifice length-to-diameter ratio is greater than 10 [17]. The jet flow of the 0.5S injector shows relatively strong flow surface perturbations compared with that of the 0.5R injector. In particular, jet flows at the injection pressure differential of 3 bar, at which cavitation occurs inside orifice, show strongly growing perturbations on the jet surface. In the case of the 0.5SS injector, cavitation is observed starting from 2 bar, and this coincides with the previous measurement discharge coefficient data. However, when the injection pressure differential becomes greater than 3 bar, hydraulic flip is observed inside orifice. When hydraulic flip occurs, white bubbles vanish and a striped pattern caused by an air tube is shown in the orifice. Moreover, in the jet flow, the strong turbulence tendency due to cavitation becomes weaker and jet flow shape becomes similar to a steady flow shape at large pressure differentials. Flow passage becomes narrow owing to the hydraulic flip phenomenon, and the ejected jet diameter becomes smaller than the orifice diameter. Actual ejected jet diameters for each condition, which were measured by direct photographs, are summarized in Table 2.

Through mass-flow-rate measurements and injector internal/external flow direct photographs, the characteristics of each flow phenomenon were compared. We tabulated variable ratios normalized by the results of the 0.5R injector in Table 3. For example, all of ratios in the 0.5R injector column are one. Comparing the mass-flow rate of the 0.5S injector in the range of 3 to 6 bar (in the case of cavitation) with the mass-flow rate of the 0.5R injector, the

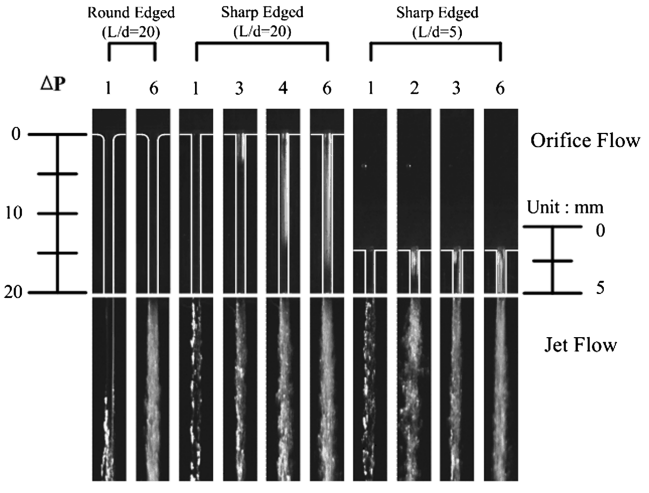

Fig. 4 Internal flows and external flows of 0.5 mm injector orifices.

Table 2 Jet diameters of 0.5 mm injectors

Flow (injector, ΔP)	Jet diameter, mm
Steady (0.5R, 1 ~ 6 bar)	0.5
Cavitation (0.5S, 3 ~ 6 bar)	0.5
Hydraulic flip (0.5SS, 4 ~ 6 bar)	0.44

Table 3 Parameter ratios compared with results of 0.5R injector

Flow (injector, ΔP)	Steady (0.5R, 1 ~ 6 bar)	Cavitation (0.5S, 3 ~ 6 bar)	Hydraulic flip (0.5SS, 4 ~ 6 bar)
$\dot{m}/\dot{m}_{\text{non}}$	1	0.75 ~ 0.80	0.68
A/A_{non}	1	1	0.77
$v_f/v_{f,\text{non}}$	1	0.75 ~ 0.80	0.86

mass-flow-rate ratio is about 0.75 to 0.80. At this time, from the direct photography confirming jet diameters, the jet diameter was found to be the same as the injector orifice diameter of 0.5 mm. Hence, the jet velocity of this case is about 0.75–0.80 times as large as that of the steady flow, because the jet velocity is proportional to the mass-flow rate if the jet cross-sectional area is the same. Comparing the mass-flow rate of the 0.5*SS* injector in the range of 4 to 6 bar (in the case of hydraulic flip) with that of the 0.5*R* injector, the mass-flow-rate ratio was found to remain constant at 0.68. However, as previously stated, when the flow passage becomes smaller due to hydraulic flip, it is found that the cross-sectional area is about 0.77. Therefore, the jet velocity is estimated to be about 0.86 times as large as that of the steady flow when hydraulic flip occurs, and this velocity is larger than that of the jet velocity when cavitation occurs.

B. Analysis and Formulation of Spray Plume Region with Steady Flow Inside Orifice

In the previous section, elementary works without crossflow of air were discussed through mass-flow rate measurements and direct photography of the inside/outside of the injector orifice. Based on these results, the PLLIF technique was applied. As stated in the experimental method, fluorescence images were obtained using PLLIF, the images of which are related to the concentration of the spray. Hence, the penetration and distribution of the spray plume region are discussed using these fluorescence images in several test cases.

Before results analysis, the parameters for analyzing the spray shape from the fluorescence images must be defined. Figure 5 shows a fluorescence image obtained from PLLIF. As shown in this image, spray is distributed roundly, and it is concentrated near the center of the spray shape. In particular, the maximum mass concentration passes through the right and left positions, a little away from the center, and then through the middle of the spray. High-velocity airflow coming with the crosswise direction collides with the liquid column of fuel jet and flows on the surface of this column. This liquid column close to the airflow is also affected by shear force. Because of this force, a counter-rotating vortex pair occurs inside the liquid column. As the spray expands toward the downstream direction, a kidney shape based on the vortex pair becomes more apparent. In Fig. 5, the parameters in the fluorescence image related to penetration heights and width are defined. The x coordinate is defined in the downstream direction from the orifice exit, the y coordinate is defined in the vertical direction from the orifice exit, and the z coordinate is defined in the direction of the width of the spray. The origin of the coordinate system is placed at the orifice exit. The valid boundary of the spray region was also determined; the boundary contains 92.5% of the total sum of light intensities in the fluorescence image in order to compare with the PDPA results of Wu et al. [1]. With a defined coordinate system and spray region, the maximum penetration height

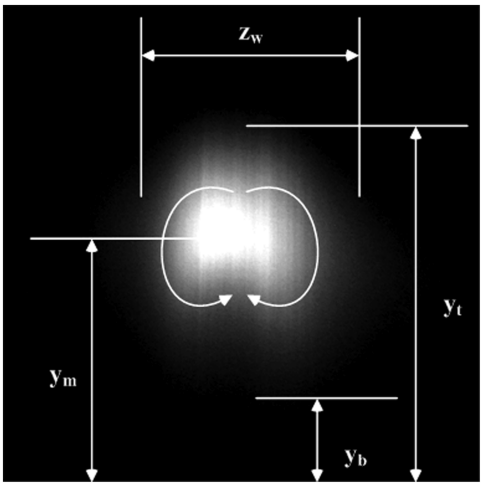

Fig. 5 Spray shape obtained from PLLIF.

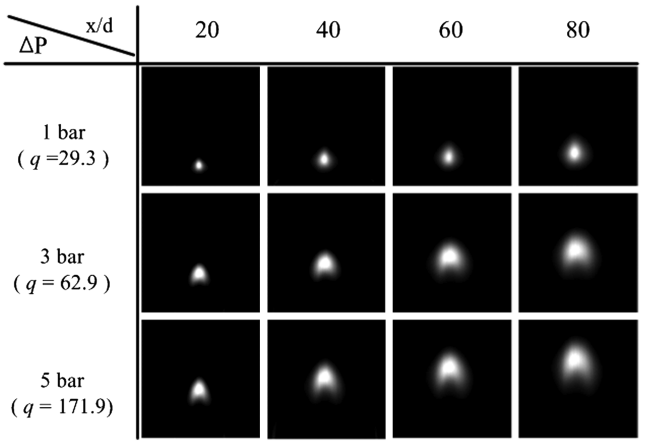

Fig. 6 Spray plume structure images obtained at each downstream location with increase of injection pressure differential for the 0.5*R* injector.

of the spray is marked as y_t and the maximum light intensity height in the fluorescence image is marked as y_m, because the place with the maximum light intensity means that the place passes through the maximum mass concentration and the lower penetration height of the spray (in other words, the bottom height of the defined region) is marked as y_b. Lastly, the spray width is marked as z_w. Figure 6 shows a series of spray plume structure images obtained at each downstream location with the increase of the injection pressure differential for the 0.5*R* injector. As the pressure differential increases, the jet velocity of the stimulant fuel increases and the penetration, which is affected by the jet velocity, also increases. Furthermore, as the pressure differential increases, the spray plume area becomes broader. This result comes from the increment of mass-flow rate, which makes the spray area increase. At the injection pressure differential of 1 bar, the penetration seldom increases in the downstream direction. However, at higher injection pressure differentials, the penetration increases in the downstream direction. At this time, unlike penetration, spray width does not noticeably increase, most likely because of the long distance that is needed to bend a spray trajectory. On the other hand, because a liquid jet having almost the same width ejects due to the initial orifice diameter, the spray width does not expand and is only affected by the counter-vortex pair. Hence, the spray width increases by a small amount compared with the spray penetration in the same condition.

After defining the parameters related penetration and width, quantitative analysis was carried out using these parameters. Wu et al. [1] analyzed the spray characteristics in spray plume region with stable flow. Using this result, we verified the reasonableness of our data for stable flow. Our data and correlations of Wu et al. [1] are compared in Figs. 7a and 7b. Figure 7a shows data for the pressure differential of 2 bar (that is, a liquid–air momentum flux ratio of 62.8), and Fig. 7b shows data for the pressure differential of 5 bar (that is, a liquid–air momentum flux ratio of 171.9). In the condition of the latter graph, if the normalized length in the x direction x/d exceeds 100, the maximum penetration of the spray plume reaches the top wall of the test section so that the maximum penetration height y_t over 100 of x/d cannot be used. Wu et al. carried out an experiment with the liquid–air momentum flux ratio ranging from 5.3 to 59.1, and this experimental condition was close to our condition of under 2 bar of pressure differential. Our result with 2 bar of pressure differential was in good agreement with the correlation proposed by Wu et al. [1]. On the other hand, for the liquid–air momentum flux ratio of 171.9 ($\Delta P = 5$ bar), the maximum penetration height data show considerable agreement with the correlation proposed by Wu et al. [1]; however, the maximum mass concentration height data show a considerable difference [1]. This difference comes from the fact that they carried out their experiment and analysis using the PDPA with limited test ranges of an x/d of 200, 300, and 500. Lastly, the bottom height data of the spray plume in both conditions remained almost constant as the x/d increased.

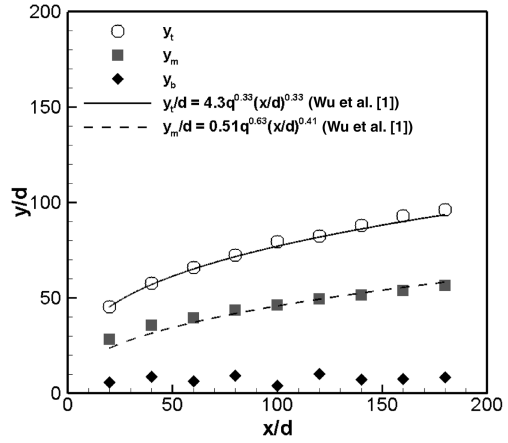

a)

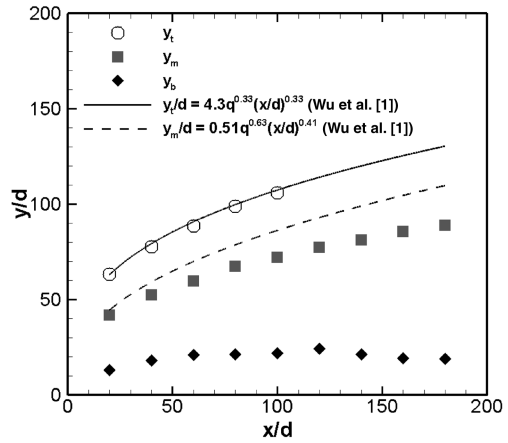

b)

Fig. 7 Comparison with correlations of Wu et al. [1]: a) $\Delta P = 2$ bar, $q = 62.8$, and b) $\Delta P = 5$ bar, $q = 171.9$.

Typically, at the leeward surface of liquid column, this column directly disintegrates with tiny droplets and the tiny droplets flow toward downstream; this is called surface breakup. Furthermore, large droplets are placed in the higher penetration region, but tiny droplets are spread out near the bottom wall. This phenomenon is thought to give an almost constant lower height of the spray plume.

Figure 8 shows the penetration correlations of the spray plume for steady flow inside the orifice normalized by the orifice diameter d and liquid–air momentum flux ratio q, where the injection jet velocities were calculated from Eq. (1). Wu et al. [1] suggested that the difference between the liquid column region and the spray plume region comes from the shape difference between the liquid column and the liquid droplet undergone drag force in the trajectory analysis described in the empirical method. Hence, they used the drag coefficients corresponding to these shapes. Based on this work, correlations were formulated based on the idea that the orifice diameter d and the liquid–air momentum flux ratio q determine the spray distribution at constant liquid viscosity and Weber number conditions. Equation (2), suggested by Wu et al. [8], is used in order to maintain the consistency of the liquid column region data and spray plume region data:

$$\frac{y}{dq} = C\left[\frac{x}{dq}\right]^n \tag{2}$$

Measured data with maximum penetration height y_t, maximum mass concentration height y_m, and lower height y_b are marked as rectangle, triangle, and circle, respectively. Three Eqs. (3–5) with each height were obtained with similar forms of Eq. (2):

$$y_t/dq = 0.825(x/dq)^{0.50} \tag{3}$$

$$y_m/dq = 0.573(x/dq)^{0.41} \tag{4}$$

$$y_b/dq = 0.224(x/dq)^{0.23} \tag{5}$$

$$y_m/d = 0.51q^{0.63}(x/d^{0.41}) \tag{6a}$$

$$y_m/dq = 0.51\left(x/d^{0.41}q^{0.37}\right) \tag{6b}$$

$$z_w/dq = 0.560(x/dq)^{0.60} \tag{7}$$

It is found that y_t/dq is proportional to $(x/dq)^{0.50}$, as shown in Eq. (3), This equation shows the same exponent as the equation $y_t/d = 1.37\sqrt{q(x/d)}$ and the equation $y/dq = 1.297(x/dq)^{0.509}$, which are suggested by Wu et al. [8] and Ahn et al. [19], respectively. This implies that the difference between the characteristics of the liquid column region and the spray plume region results from the difference of the drag coefficients according to the liquid shapes. Equation (6b) is obtained by dividing Eq. (6a), which was suggested by Wu et al. [1], into the liquid–air momentum flux ratio q; this equation is similar with Eq. (4), obtained by our results. From Eq. (6b), the problem that the expected trajectory curve gives larger values than the real values for larger values of the liquid–air momentum flux ratio is found. Although the difference between $q^{0.37}$ and $q^{0.41}$ for small values of q is not considerable, there is a remarkable difference for the large values of q. Lower height trajectory data also follow the same equation shape with Eq. (2), although a measurement error exists due to the tiny droplet size.

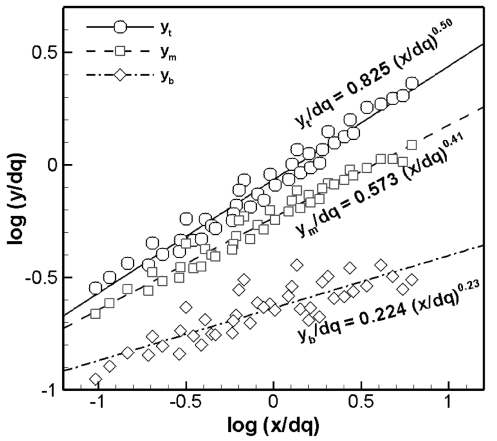

Fig. 8 Spray plume trajectory at a steady flow: penetration correlations in the cases of y_t/dq, y_m/dq, and y_b/dq.

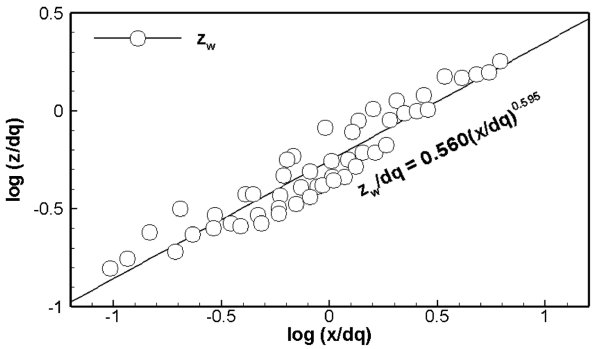

Fig. 9 Spray plume trajectory at a steady flow: width correlations in the cases of y_t/dq, y_m/dq, and y_b/dq.

Figure 9 presents a correlation for the spray width. In the same way, the width of the spray plume z_w can also be expressed as Eq. (7) of x/dq and z/dq. We derived the correlation for the width of the spray plume for steady flow from the maximum length of the spray plume width, unlike Wu et al. [1], who derived the correlation of width as a function of the injection nozzle area to the spray plume area ratio.

C. Comparison of Penetration and Width Among Three Internal Flows Inside Orifices

Based on the spray plume characteristics in the fluorescent images obtained by the PLLIF method, we compared penetrations and widths of the spray plume region among the phenomena that can occur inside an orifice: steady flow, cavitation flow, and hydraulic flip flow. Many papers have discussed penetration, including Wu et al. [1], Smith and Mungal [28], and Inamura and Nagai [14], because penetration is a fundamental factor in the understanding of spray characteristics and structures. In Fig. 10, the measured points of steady flow, cavitation flow, and hydraulic flip flow, which include the maximum penetration height, maximum mass concentration height, and lower height, were compared. Penetrations of steady flow injected from the 0.5*R* injector are marked as rectangles, penetrations of cavitation flow injected from the 0.5*S* injector are marked as triangles, and penetrations of hydraulic flip flow injected from the 0.5*SS* injector are marked as circles. Moreover, the solid lines, dashed–dotted lines, and dashed–dotted–dotted lines indicate the maximum penetration height, maximum mass concentration height, and lower height, respectively. Figure 10a is a comparison of each penetration among each flow phenomena at an injection pressure differential of 3 bar. For the maximum penetration height and maximum mass concentration height in the spray plume region, it is shown that each penetration curve is located in order of steady flow, hydraulic flip flow, and cavitation flow. On the other hand, it is observed that the lower height curve of each phenomenon in the spray plume region remains almost constant, regardless of the flow condition inside the orifice. As addressed, this is because the dominant breakup mechanism of the lower region is the surface breakup at the leeward surface of the liquid column. This penetration difference of the maximum penetration height and maximum mass concentration height, like the jet velocity results in Table 3, is caused by the jet velocity in the case of hydraulic flip flow that is larger than that in the case of cavitation flow despite the smaller mass-flow rate. Figure 10b is a comparison of each penetration among each flow phenomena at an injection pressure differential of 6 bar. Patterns identical to the results in Fig. 10a are observed in this figure; however, the penetration differences of the maximum penetration height and the maximum mass concentration height among the different flow phenomena are larger, and those of the lower height are also slightly affected by the large injection pressure differential. This result shows that unstable flow due to cavitation or hydraulic flip strongly influences spray plume characteristics as the injection pressure differential increases. Similarly, the spray plume width was compared for each flow condition inside the orifice. Figures 11a and 11b are comparisons of width among each flow phenomena for the injection pressure differentials of 3 and 6 bar, respectively. It is observed that the spray plume width curves in both graphs show few differences among the phenomena, which implies that the width is only slightly affected by the jet velocities of each phenomenon. Moreover, the spray plume width increases with similar values among the flow conditions when the liquid column diameters are the same. Between the values of Fig. 11a and those of Fig. 11b, all of the curves are very similar, despite the different injection pressure differential. This result also implies that spray plume width is not related to the injection velocity, but it is strongly related to the liquid column diameter.

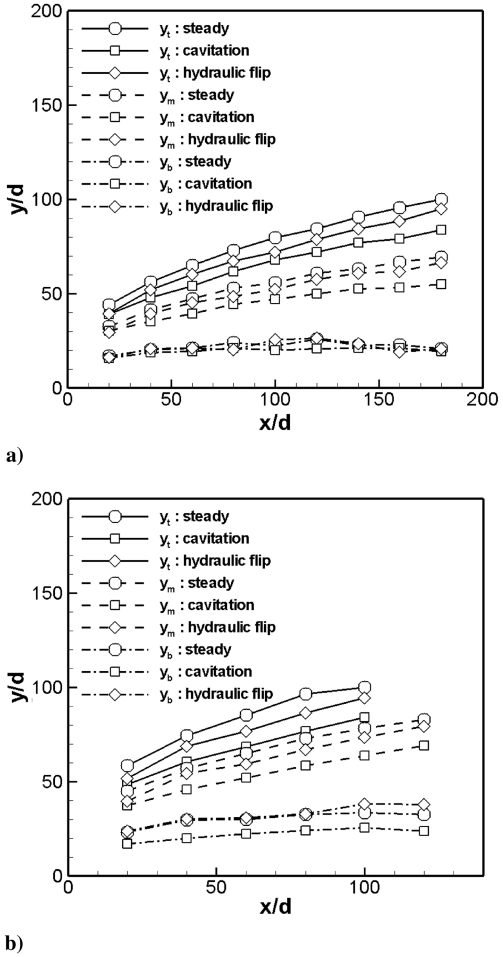

Fig. 10 Penetration comparison with each case of steady flow, cavitation flow, and hydraulic flip flow: a) $\Delta P = 3$ bar and b) $\Delta P = 5$ bar.

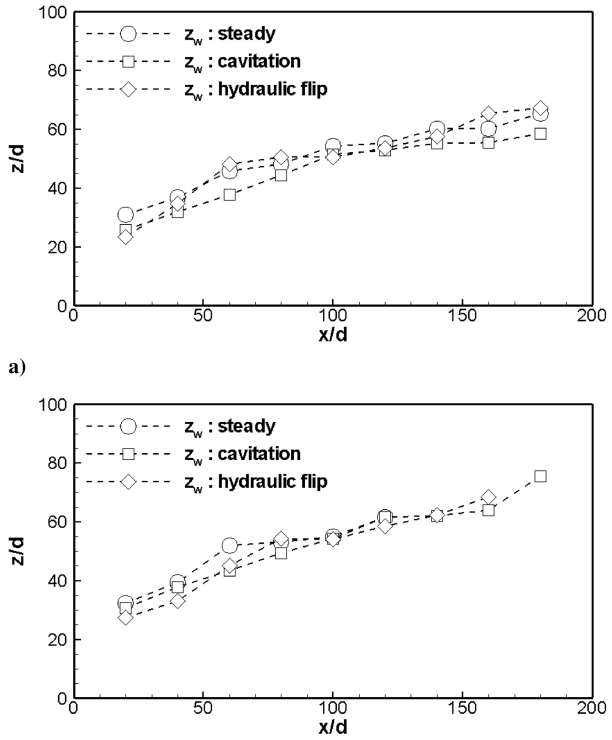

Fig. 11 Width comparison with each case of steady flow, cavitation flow, and hydraulic flip flow: a) $\Delta P = 3$ bar and b) $\Delta P = 5$ bar.

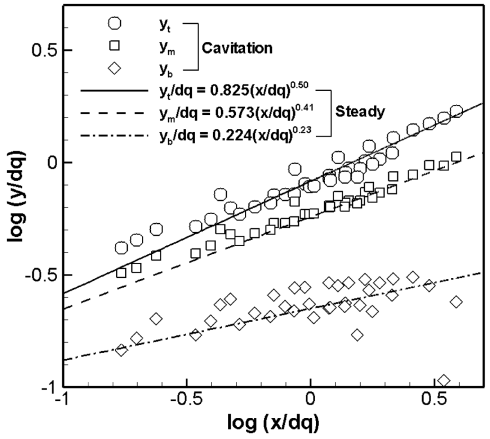

a)

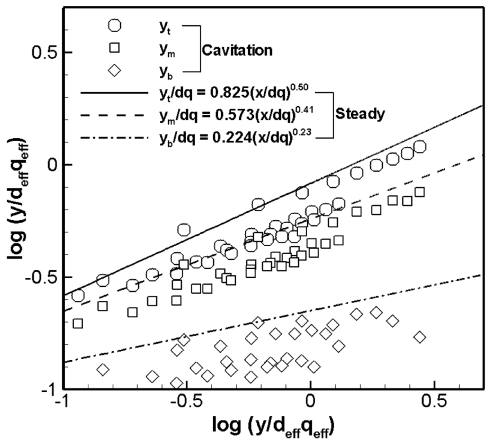

b)

Fig. 12 Penetration correlation at cavitation flow: a) using d and q, and b) using d_{eff} and q_{eff}.

D. Effective Parameters Related to Cavitation Flow and Hydraulic Flip Flow Inside Orifice

In the previous section, correlations for penetrations and width in the spray plume region with steady flow inside the orifice were suggested. Here, we discuss whether these correlations can be applied to cases of cavitation flow or hydraulic flip flow. Then, if they can be used, we determine what adjustment factors must be introduced into these correlations, because it is very inconvenient to introduce correlations for each phenomenon inside the orifice, even though there is a remarkable similarity called transverse injection. Figure 12 shows a comparison between the data with cavitation flow inside the orifice and the correlations obtained for steady flow inside the orifice. The symbols represent the data obtained from the fluorescence images of cavitation flow, and the lines represent the correlations obtained for steady flow. Figure 12a shows the normalized values, which are obtained by dividing the penetration data by the orifice diameter d and the liquid–air momentum flux ratio q, including the jet velocity in the case of cavitation flow. Figure 12b shows the normalized values, which are obtained by dividing the penetration data by the effective orifice diameter d_{eff} and the effective liquid–air momentum flux ratio q_{eff}, including the effective jet velocity from the equations of Schmidt and Corradini [29]:

$$u_{\text{eff}} = \frac{2C_c(P_1 - P_v) - (P_2 - P_v)}{C_c\sqrt{2\rho_l(P_1 - P_v)}} \tag{8}$$

$$A_{\text{eff}} = \frac{2C_c^2(P_1 - P_v)}{2C_c(P_1 - P_v) - (P_2 - P_v)}A \tag{9}$$

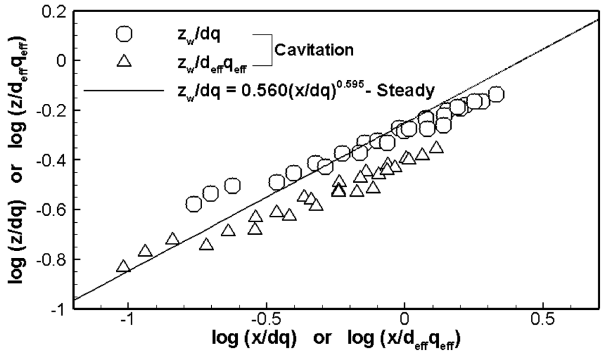

Fig. 13 Width correlation at cavitation flow: a) using d and q, and b) using d_{eff} and q_{eff}.

The comparison between Figs. 12a and 12b, in the case of cavitation flow inside the orifice, shows that the normalized data by the given orifice diameter and liquid–air momentum flux ratio using the calculated jet velocity are more appropriate than those obtained from the effective factors calculated from the equations suggested by Schmidt and Corradini [29]. The same conclusion can be applied to the spray plume width for cavitation flow inside the orifice. Figure 13 shows the width data normalized by the orifice diameter d and liquid–air momentum flux ratio q, and the data normalized by the effective orifice diameter d_{eff} and the effective liquid–air momentum flux ratio q_{eff}, respectively. For the spray plume width, normalized data obtained with the given orifice diameter and the liquid–air momentum flux ratio using calculated jet velocity are also more appropriate than those obtained with the effective factors calculated from the equations suggested by Schmidt and Corradini [29]. The results for cavitation flow inside the orifice coincide with the results of Ahn et al. [19] for the liquid column region.

While hydraulic flip is caused by cavitation, it has different appearances. Using the same method related to cavitation flow, the effective factors for normalizing the spray plume characteristics were compared. Ahn et al. [19] suggested experimental correlations of the liquid column for the hydraulic flip condition inside the orifice using the following equations:

$$A_{\text{eff,hyd}} = A\frac{C_{d,\text{hyd}}}{C_{d,\text{non}}} \tag{10}$$

$$V_{\text{eff,hyd}} = V_f\frac{A}{A_{\text{eff,hyd}}} \tag{11}$$

In these equations, C_d is the discharge coefficient obtained from the mass-flow-rate measurements and $C_{d,\text{non}}$ is the discharge coefficient measured just before the occurrence of cavitation. Moreover, Eqs. (8) and (9) [29], which were used to determine the effective factor in the cavitation condition, were also used to determine the effective factor for normalizing spray plume characteristics. Figure 14 shows the penetration graphs: in Fig. 14a, no effective factor was used for normalizing the penetrations in the spray plume region, and in Figs. 14b and 14c, the effective factors suggested by Ahn et al. [19] and Schmidt and Corradini [29] were introduced for normalizing penetrations. The comparisons of Figs. 14a–14c for hydraulic flip flow inside the orifice showed that the normalized data by using the effective factors calculated from the equations suggested by Ahn et al. [19] and Schmidt and Corradini [29] are more appropriate than those by using given orifice diameter and liquid–air momentum flux ratio using the calculated jet velocity. The equations of Ahn et al. [19] were created by experiment, and the equations of Schmidt and Corradini [29] were introduced by theoretical analysis. With the equations of Ahn et al. [19], the maximum penetration height data show a good agreement with the correlation for steady flow, but other height data show some differences. On the other hand, with the equations of Schmidt and Corradini [29], all penetration data are

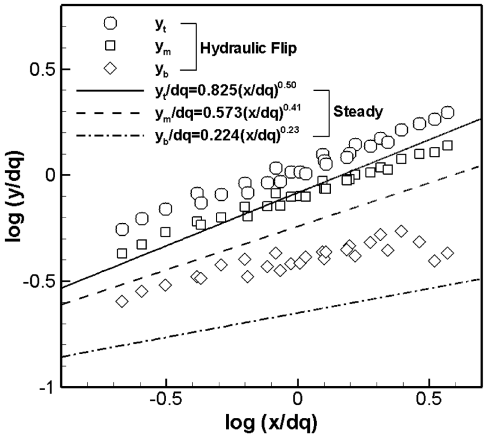

a)

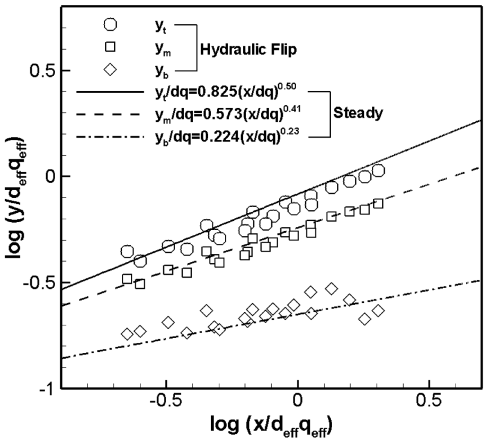

b)

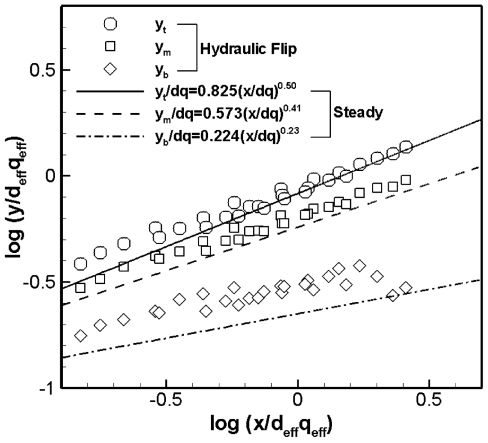

c)

Fig. 14 Penetration correlations at hydraulic flip flow: a) using d and q, b) using d_{eff} and q_{eff} (Ahn et al. [19]), and c) using d_{eff} and q_{eff} (Kihm et al. [16]).

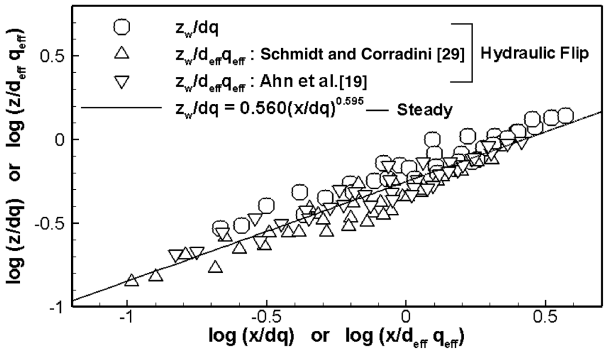

Fig. 15 Width correlations at hydraulic flip flow using d and q and these effective factors.

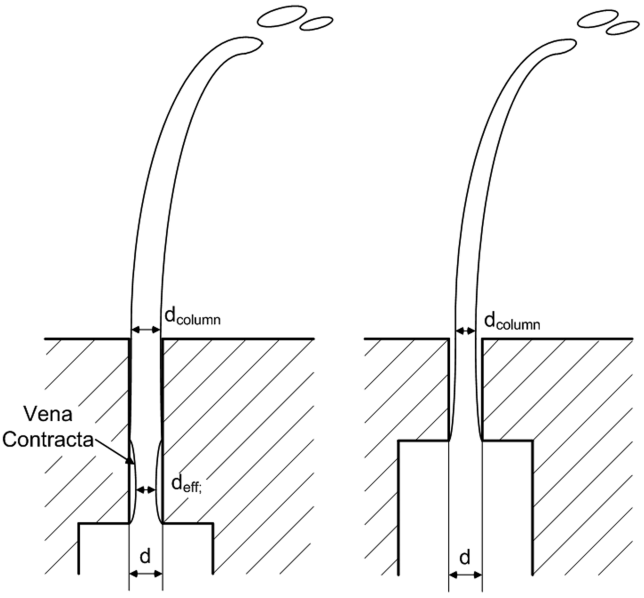

Fig. 16 Schematics of how orifice internal disturbance influence to transverse injection: a) cavitation and b) hydraulic flip.

matched with the penetration correlations of steady flow. However, these equations have a fault: neither the surface friction of the liquid gas nor the boundary layer effect is considered in the theoretical analysis. Figure 15 shows the width graph and is arranged in the same order as Fig. 14. There is no remarkable difference between the case applied with effective factors for normalization and a case not applied with effective factors. However, the case in which the equation of Ahn et al. [19] is used as the effective factors for normalizing the spray plume width shows good agreement with the width curve for the steady flow in detail. Hence, for spray plume width, the introduction of effective factors is also appropriate. This result coincides with the results of Ahn et al. [19] in connection with the liquid column region. It is necessary to consider the reason why the effective factors introduced are different between cavitation and hydraulic flip. Figure 16 is a schematic near the orifice for each flow condition inside the orifice: Fig. 16a is a schematic of cavitation flow, and Fig. 16b is a schematic of hydraulic flip flow. As shown in Fig. 16a, in the case of cavitation flow, a vena contracta occurs at the orifice entrance, but the bubbles caused by the vena contracta are kept inside the orifice. Hence, the diameter of the liquid column is almost identical to the orifice diameter. The fact that the given orifice diameter d and the liquid–air momentum flux ratio q using the calculated jet velocity are appropriate for normalizing the spray plume characteristics in the cavitation flow inside the orifice implies that the spray structure is governed by the diameter of the liquid column and the average jet velocity corresponding to the diameter of the liquid column. In other words, the effective diameter and velocity suggested by Schmidt and Corradini [29] are related to the narrow flow passage due to the vena contracta, and these factors are not the same as the factors of the liquid column at the orifice exit. Similarly, the diameter of the liquid column is smaller than that of the orifice due to an air envelope in the case of hydraulic flip flow inside the orifice; for this reason, the given orifice diameter and the jet velocity obtained from the orifice diameter are not adequate for normalizing spray plume characteristics. Therefore, it is necessary to introduce effective factors.

IV. Conclusions

The main objective of this study was to determine the spray plume characteristics of liquid jets in subsonic crossflows and to investigate the effect of the orifice internal flow on the spray plume characteristics. From the experimental results, the following conclusions can be drawn.

From the mass-flow-rate measurement, when the orifice internal flow is steady, the discharge coefficients increase linearly with respect to the Reynolds number as the pressure differentials increase. However, when the internal flows are unsteady, the coefficients do not behave like the results of steady flow. In the case of cavitation flow, the discharge coefficients decrease gradually due to the narrow flow passage caused by the cavitation. Also, in the case of hydraulic flip flow, the coefficient pattern shows a sudden drop and smaller constant values than those of the steady flow due to the narrow passage.

Similarly, through direct photography, no phenomena are found inside the orifices using the round-edged orifice designed for inducing steady flow, and jet flow shows no significant changes. However, in the case of unsteady flows, orifice internal flows became more unsteady as the pressure difference was increased. This unsteady phenomena occurred as cavitation and hydraulic flip, depending on whether the internal liquid flow was detached or not. The jet shape of cavitation flow had a large wrinkle, but that of hydraulic flip flow showed steady behavior like that of steady flow. However, each of the unsteady flows had a smaller discharge coefficient than that of the steady flow. Accordingly, steady flow yielded the largest values of penetrations and width.

The PLLIF method was carried out to obtain the correlation of the spray structure parameter, penetration, and width. It is suggested that spray penetrations and width can be generalized with orifice diameter d and liquid–air momentum flux ratio q, as in the following Eqs. (4), (5), (6a), and (8). These equations can cover the range of the broad liquid–air momentum flux ratio from 20.6 to 206.8.

Spray plume trajectory is determined by the liquid column diameter of the orifice exit and the liquid–air momentum flux ratio using the jet velocity at the orifice exit rather than the orifice exit diameter and the liquid–air momentum flux ratio calculated by using nominal diameter. This conclusion can be also confirmed from the result that shows that the penetrations of each phenomenon have considerable differences due to the difference of vertical jet velocities; however, the widths of each phenomena show very similar values caused by little differences of the jet velocities in the direction of the width of the spray. Therefore, if cavitation flow occurs, it is better to use the nominal diameter and liquid–air momentum flux ratio, because the liquid column diameters of the orifice exit are the same as the nominal diameters due to flow reattachment at the orifice exit. On the other hand, if hydraulic flip flow occurs, it is better to use the effective diameter and liquid–air momentum flux due to the discrepancy between the liquid column diameter and the nominal orifice diameter. This discrepancy makes the jet velocity faster and jet diameter smaller, so that the spray penetrations become higher and the spray width becomes narrower.

Acknowledgment

This research has been supported by the Institute of Advanced Aerospace Technology, Seoul National University.

References

[1] Wu, P. K., Kirkendall, K. A., Fuller, R. P., and Najad, A. S., "Spray Structures of Liquid Jets Atomized in Subsonic Crossflows," *Journal of Propulsion and Power*, Vol. 14, No. 2, 1998, pp. 173–182. doi:10.2514/2.5283

[2] Schetz, J. A., Kush, E. A. Jr., and Joshi, P. B., "Wave Phenomena in Liquid Jet Breakup in a Supersonic Crossflow," *AIAA Journal*, Vol. 18, No. 7, 1980, pp. 774–778. doi:10.2514/3.7687

[3] Ingebo, R. D., "Aerodynamic Effects of Combustor Inlet-air Pressure on Fuel Jet Atomization," AIAA Paper 1984-1320, 1984.

[4] Schetz, J. A., and Padhye, A., "Penetration and Breakup of Liquids in Subsonic Airstreams," *AIAA Journal*, Vol. 15, No. 10, 1977, pp. 1385–1390. doi:10.2514/3.60805

[5] Ingebo, R. D., "Penetration of Drops into High-Velocity Airstreams," NASA TM X-1363, 1967.

[6] Chelko, L. J., "Penetration of Liquid Jets into a High-Velocity Air Stream," NACA RM E50F21, 1950.

[7] Chen, T. H., Smith, C. R., Schommer, D. G., and Nejad, A. S., "Multi-Zone Behavior of Transverse Liquid Jet in High-Speed Flow," AIAA Paper 1993-0453, 1993.

[8] Wu, P. K., Kirkendall, K. A., Fuller, R. P., and Najad, A. S., "Breakup Processes of Liquid Jets in Subsonic Crossflows," *Journal of Propulsion and Power*, Vol. 13, No. 1, 1997, pp. 64–73. doi:10.2514/2.5151

[9] Sallam, K. A., Aalburg, C., and Faeth, G. M., "Breakup of Round Nonturbulent Liquid Jets in Gaseous Crossflow," *AIAA Journal*, Vol. 42, No. 12, 2004, pp. 2529–2540. doi:10.2514/1.3749

[10] Stenzler, J. N., Lee, J. G., Santavicca, D. A., and Lee, W., "Penetration of Liquid Jets in a Cross-Flow," *Atomization and Sprays*, Vol. 16, Iss. 8, 2006, pp. 887–906. doi:10.1615/AtomizSpr.v16.i8.30

[11] Baranovsky, S. I., and Schetz, J. A., "Effect of Injection Angle on Liquid Injection in Supersonic Flow," *AIAA Journal*, Vol. 18, No. 6, 1980, pp. 625–629. doi:10.2514/3.50798

[12] Fuller, R. P., Wu, P. K., Kirkendall, K. A., and Nejad, A. S., "Effects of Injection Angle on Atomization of Liquid Jets in Transverse Airflow," *AIAA Journal*, Vol. 38, No. 1, 2000, pp. 64–72. doi:10.2514/2.923

[13] Kim, M. K., Song, J., Hwang, J., and Yoon, Y., "Effects of Canted Injection Angles on the Spray Characteristics of Liquid Jets in Subsonic Crossflows," *Atomization and Sprays*, Vol. 20, No. 9, 2010, pp. 749–762.

[14] Inamura, T., and Nagai, N., "Spray Characteristics of Liquid Jet Traversing Subsonic Airstreams," *Journal of Propulsion and Power*, Vol. 13, No. 2, 1997, pp. 250–256. doi:10.2514/2.5156

[15] Oda, T., and Hiroyasu, H., "Breakup Model of Liquid Jet Across a High-Speed Air Stream," *Proceedings of the 9th Annual Conference on Liquid Atomization and Spray Systems*, San Francisco, CA, Inst. for Liquid Atomization and Spray Systems, Irvine, CA, 1996, pp. 99–103.

[16] Kihm, K. D., Lyn, G. M., and Son, S. Y., "Atomization of Cross-Injecting Sprays into Convective Air Stream," *Atomization and Sprays*, Vol. 5, Nos. 4–5, 1995, pp. 417–433.

[17] Nurick, W. H., "Orifice Cavitation and Its Effect on Spray Mixing," *Journal of Fluids Engineering*, Vol. 98, No. 4, 1976, pp. 681–687. doi:10.1115/1.3448452

[18] Tamaki, N., Shimizu, M., Nishida, K., and Hiroyasu, H., "Effects of Cavitation and Internal Flow on Atomization of a Liquid Jet," *Atomization and Sprays*, Vol. 8, No. 2, 1998, pp. 179–197.

[19] Ahn, K., Kim, J., and Yoon, Y., "Effects of Orifice Internal Flow on Transverse Injection into Subsonic Crossflows: Cavitation and Hydraulic Flip," *Atomization and Sprays*, Vol. 16, No. 1, 2006, pp. 15–34. doi:10.1615/AtomizSpr.v16.i1.20

[20] Talley, D. G., Verdieck, J. F., Lee, S. W., McDonell, V. G., and Samuelsen, G. S., "Accounting for Laser Sheet extinction in Applying PLLIF to Sprays," 34th Aerospace Sciences Meeting and Exhibit, Reno, NV, AIAA Paper 1996-0469, 1996.

[21] Koh, H., Jung, K., Yoon, Y., Lee, K., and Jeong, K. S., "Development of Quantitative Measurement of Fuel Mass Distribution Using Planar Imaging Technique," *Journal of Visualization*, Vol. 9, No. 2, 2006, pp. 161–170. doi:10.1007/BF03181759

[22] Jung, K., Koh, H., and Yoon, Y., "Assessment of Planar Liquid-Laser-Induced Fluorescence Measurements for Spray Mass Distributions of Like-Doublet Injectors," *Measurement Science and Technology*, Vol. 14, No. 8, 2003, pp. 1387–1395. doi:10.1088/0957-0233/14/8/326

[23] Crane, R., *A Simplified Approach to Image Processing*, Prentice–Hall, Upper Saddle River, NJ, 1997, pp. 206–212.

[24] Talley, D. G., Thamban, T. S., McDonell, V. G., and Samuelsen, G. S., "Laser Sheet Visualization of Spray Structure," *Recent Advances in Spray Combustion: Spray Combustion Measurements and Model Simulation*, Vol. 2, Progress in Astronautics and Aeronautics, AIAA, Washington, D.C., 1995, pp. 113–141.

[25] Jung, K., Lim, B., and Yoon, Y., "Comparision of Mixing Characteristics of Unlike Triplet Injectors Using Optical Patternator," *Journal of Propulsion and Power*, Vol. 21, No. 3, 2005, pp. 442–449.
doi:10.2514/1.12884
[26] Lide, D. R., *Handbook of Chemistry and Physics*, CRC Press, Boca Raton, FL, 1994, pp. 6–198.
[27] Lefebvre. A. H., *Atomization and Sprays*, Hemisphere, Philadelphia, 1989, p. 158.
[28] Smith, S. H., and Mungal, M. G., "Mixing, Structure and Scaling of the Jet in Crossflow," *Journal of Fluid Mechanics*, Vol. 357, 1998, pp. 83–122.
doi:10.1017/S0022112097007891
[29] Schmidt, D. P., and Corradini, M. L., "Analytical Prediction of the Exit Flow of Cavitating Orifices," *Atomization and Sprays*, Vol. 7, No. 6, 1997, pp. 603–616.

D. Talley
Editor-in-Chief